Control of ciliary transcriptional programs during spermatogenesis by antagonistic transcription factors

Weihua Wang[1,4]✉, Junqiao Xing[1,4], Xiqi Zhang[2,4], Hongni Liu[1], Haochen Jiang[1], Cheng Xu[1], Xue Zhao[1], Zhangfeng Hu[1,2,3]✉

[1]Wuhan Institute of Biomedical Sciences, School of Medicine, Jianghan University, Wuhan, 430056 Hubei, China

[2]School of Life Sciences, Jianghan University, Wuhan, 430056 Hubei, China

[3]Hubei Key Laboratory of Environmental and Health Effects of Persistent Toxic Substances, Jianghan University, Wuhan, 430056 Hubei, China

[4]These authors contributed equally: Weihua Wang, Junqiao Xing, Xiqi Zhang

✉e-mail: wangwh2019@163.com; huzhangfenghzf@163.com

Abstract

Existence of cilia in the last eukaryotic common ancestor (LECA) raises a fundamental question in biology: how the transcriptional regulation of ciliogenesis has evolved? One conceptual answer to this question is by an ancient transcription factor regulating ciliary gene expression in both unicellular and multicellular organisms, but examples of such transcription factors in eukaryotes are lacking. Previously, we showed that an ancient transcription factor XAP5 is required for flagellar assembly in *Chlamydomonas*. Here, we show that XAP5 and XAP5L are two conserved pairs of antagonistic transcription regulators that control ciliary transcriptional programs during spermatogenesis. Male mice lacking either XAP5 or XAP5L display infertility, as a result of meiotic prophase arrest and sperm flagella malformation, respectively. Mechanistically, XAP5 positively regulates the ciliary gene expression by activating the key regulators including FOXJ1 and RFX families during the early stage of spermatogenesis. In contrast, XAP5L negatively regulates the expression of ciliary genes via repressing these ciliary transcription factors during the spermiogenesis stage. Our results provide new insights into the mechanisms by which temporal and spatial transcription regulators are coordinated to control ciliary transcriptional programs during spermatogenesis.

Introduction

Cilia and flagella are evolutionarily conserved hair-like microtubule organelles that project from the surfaces of most eukaryotic cells(Derderian, Canales, & Reiter, 2023; Mitchell, 2017). They play essential roles in sensory reception, signal transduction and cell movement(Goetz & Anderson, 2010; Nachury & Mick, 2019; Singla & Reiter, 2006). The dysfunction of cilia in humans leads to an emerging class of genetic diseases called ciliopathies classified into first-order and second-order ciliopathies(Ishikawa & Marshall, 2011; Lovera & Lüders, 2021; Reiter & Leroux, 2017). First-order ciliopathies are caused by aberrations in ciliary proteins, and second-order ciliopathies occur due to defects in non-ciliary proteins, such as transcription factors, that are required for cilia formation and function(Reiter & Leroux, 2017).

Cilia are complex organelles and are dynamically regulated during development and the cell cycle(Eggenschwiler & Anderson, 2007; Kasahara & Inagaki, 2021; Santos & Reiter, 2008). The transcriptional regulation of ciliary genes must be precisely coordinated during ciliogenesis(Choksi, Lauter, Swoboda, & Roy, 2014; Collins, Ventrella, & Mitchell, 2021; Lewis & Stracker, 2021; Thomas et al., 2010). In metazoans, several transcription factors, including FOXJ1 and RFXs, have been shown to be involved in directing the expression of ciliary genes(Stubbs, Oishi, Izpisua Belmonte, & Kintner, 2008; Swoboda, Adler, & Thomas, 2000; Yu, Ng, Habacher, & Roy, 2008). These key ciliary transcription factors show dynamic expression patterns during development and differentiation(Stubbs et al., 2008; Swoboda et al., 2000; Yu et al.,

64 2008). However, how these key transcriptional programs are spatially and temporally
65 controlled by cell type-specific transcription factors and signaling pathways in order to
66 activate specific target ciliary genes and generate diverse cilia is largely unknown.

67 Despite transcriptional regulation of ciliary genes is required for ciliogenesis in both
68 unicellular and multicellular organisms, the underlying mechanism mediating ciliary gene
69 expression may be fundamentally different, as the two major transcription factors, FOXJ1
70 and RFXs, are absent from many unicellular organisms(Chu, Baillie, & Chen, 2010; Li et
71 al., 2018; Piasecki, Burghoorn, & Swoboda, 2010; Vij et al., 2012). Cilia and ciliary
72 genes have been highly conserved throughout evolution, suggesting that the regulation of
73 ciliary genes could be programmed by yet undiscovered transcriptional mechanisms,
74 which possibly coevolved with multicellularity. Recently, an ancient transcription factor,
75 XAP5, is found to regulate ciliary gene expression in a unicellular organism,
76 *Chlamydomonas reinhardtii*(Li et al., 2018). XAP5 is highly conserved among different
77 species and is widely expressed across tissues(Martin-Tryon & Harmer, 2008;
78 Mazzarella, Pengue, Yoon, Jones, & Schlessinger, 1997). In vertebrates, *XAP5-like*
79 (*XAP5L*) with an intronless open reading frame originated in Therians via
80 retrotransposition of the ancestral *XAP5*, and it is highly expressed during
81 spermatogenesis(Sedlacek et al., 1999; A. Zhang et al., 2011). However, whether XAP5
82 and XAP5L play essential roles in cilia development in multicellular organisms remains
83 unknown.

84 Here, we show that XAP5/XAP5L are antagonistic transcription factors required for

85 ciliary transcriptional programs during spermatogenesis. XAP5 is widely expressed in
86 different tissues, while XAP5L is exclusively present in the testes. To explore the roles of
87 XAP5/XAP5L in ciliogenesis, we generated a *XAP5L* knockout (KO) mouse line and
88 found that *XAP5L* KO male mice are infertile due to the malformation of sperm flagella.
89 Interestingly, male mice with the loss of XAP5 protein in germ cells also exhibited
90 infertile, due to the arrest of spermatogenesis in the meiotic prophase stage. These data
91 suggest that XAP5/XAP5L play crucial roles in sperm flagellar assembly.
92 Mechanistically, XAP5 positively modulates transcriptional rewiring of ciliary genes via
93 activating the key regulators including FOXJ1 and RFXs during the early stage of
94 spermatogenesis. Conversely, XAP5L negatively regulates the transcriptional program
95 controlling ciliogenesis by repressing these ciliary transcription factors during the
96 spermiogenesis stage. Thus, ciliary transcriptional programs are spatially and temporally
97 controlled by XAP5/XAP5L antagonistic transcription factors during spermatogenesis.
98

99 **Results**

100 **XAP5 and XAP5L are indispensable for male fertility**

101 To explore the potential functions of XAP5/XAP5L during ciliogenesis *in vivo*, we
102 performed Western blot analysis to investigate the spatiotemporal expression of
103 XAP5/XAP5L in various mouse tissues. We observed that XAP5 protein was widely
104 expressed in diverse tissues and present at all stages of postnatal testes maturation,
105 whereas XAP5L protein was mainly present in the testes and its level increased

106 dramatically from postnatal day 21 (P21) and continued into adulthood (Figures 1A, B).
107 Next, we identified the specific testicular cell types expressing XAP5/XAP5L using
108 published single-cell RNA-seq data(Jung et al., 2019). XAP5 mRNA was found
109 predominantly expressed in spermatogonia, while XAP5L mRNA was observed in
110 pachytene spermatocytes, and remained until elongating spermatids (Figure 1C).
111 Consistent with the mRNA localization patterns, immunofluorescence staining showed
112 that XAP5 protein was mainly detected in the nuclei of spermatogonia, whereas XAP5L
113 protein was present in the nuclei of pachytene spermatocytes and spermatids within the
114 seminiferous tubules, and neither of XAP5 or XAP5L was detected in mature sperm
115 (Figure 1D and Figure S1).

116 To investigate the physiological function of the uncharacterized XAP5/XAP5L protein,
117 we attempted to generate global KO mice using the CRISPR-Cas9 system. We
118 successfully established a *XAP5L* KO mouse line (Figures S2A-C) and found that while
119 all *XAP5L* KO mice survived to adulthood and appeared indistinguishable from the
120 wildtype (WT) mice, *XAP5L* KO males were sterile (Figures 1E, F). Notably, generating
121 mosaic F0 founders with *XAP5* mutant allele proved challenging, and no F1 generation
122 inherited the mutant alleles from the few F0 founders in over a year of breeding
123 experiments, underscoring the critical roles of XAP5 in mouse development.
124 Subsequently, we generated floxed-*XAP5* mice and crossed them with *Stra8-GFPCre*
125 knockin mice(Lin et al., 2017) to produce *XAP5* germline-specific KO mice (*XAP5* cKO)
126 (Figures S2D-F). Similar in appearance to controls ($XAP5^{fl/Y}$), all *XAP5* cKO males were

127 also found to be sterile (Figures 1G, H). Collectively, these results suggest that
128 XAP5/XAP5L play essential roles in spermatogenesis.

129 **XAP5 and XAP5L function at different stages of spermatogenesis**

130 To uncover the cause of male infertility, we conducted gross and histological analyses of
131 the testes from WT and *XAP5L* KO mice. There were no differences in the gross
132 appearance of testis or in the weight of mouse body and testis between WT and XAP5L
133 KO mice (Figure 2A). Histological analysis did not reveal any severe abnormity in the
134 seminiferous epithelial cycle of XAP5L KO testes (Figure 2B). We then investigated the
135 motility of sperm collected from cauda epididymis, and found that total motility of sperm
136 was significantly reduced in *XAP5L* KO mice (Figure 2C and Videos S1, 2). Further
137 examination of the morphology and structure of cauda epididymal sperm in *XAP5L* KO
138 mice revealed significantly higher rates of abnormal flagella (Figures 2D-F), indicating
139 that XAP5L is crucial for flagellar assembly during spermiogenesis.

140 We also investigated the spermatogenic defects in the seminiferous tubules and
141 epididymis of *XAP5* cKO male mice. Notably, the testes of *XAP5* cKO males were
142 significantly smaller compared to WT controls at P16 and older (Figure 3A). Many
143 seminiferous tubules in P16 and older *XAP5* cKO males were vacuolated due to the
144 absence of spermatocytes and spermatids, as indicated by the lack of XY body formation
145 and the absence of PNA signal, a marker of spermatids and sperm, in *XAP5* cKO germ
146 cells (Figures 3B-D). As a consequence, no sperm were observed in the adult cauda
147 epididymides of *XAP5* cKO mice (Figure 3E). Taken together, these data indicate that

148 germ cell development in *XAP5* cKO males was arrested in meiotic prophase, and XAP5
149 is indispensable for meiotic progression during spermatogenesis.

150 **XAP5 and XAP5L function as antagonistic regulators of ciliary transcriptional**
151 **regulatory networks via regulating transcription factors**

152 To gain insight into the regulatory mechanisms of XAP5L during sperm flagellar
153 assembly, we employed RNA-seq analysis to examine mature sperm collected from the
154 cauda epididymis of WT and *XAP5L* KO adult mice. Differential expression analysis
155 identified 2093 upregulated and 267 downregulated genes in *XAP5L* KO sperm (Figure
156 S3A). Gene ontology analysis revealed that the upregulated genes were associated with
157 cilia assembly or function (Figure 4A and Figures S3B, C). When crossed with the
158 previously compiled ciliogenesis-related gene list(Nemajerova et al., 2016), the
159 upregulated genes were observed encompassing diverse structural and functional
160 components of the ciliogenic program (Table S1 and Figure S3D). Notably, several key
161 transcription factor (TF) regulators of ciliogenesis were among the upregulated genes,
162 including FOXJ1 and RFX families (Figures 4B, C and Figure S3E). Moreover, several
163 key regulators of spermatogenesis, particularly spermiogenesis, were identified, including
164 RFX2(Kistler et al., 2015; Wu et al., 2016), SOX families(Schartl et al., 2018; D. Zhang
165 et al., 2018), TAF7L(Zhou et al., 2013) and TBPL1(Martianov et al., 2001) (Figure 4B
166 and Figure S3E). Many core ciliary genes were also upregulated, such as
167 *CFAP206*(Beckers et al., 2020) and *IFT81*(Qu et al., 2020) which are critical for male
168 fertility (Figure S3E), consistent with the tight coregulation between spermiogenesis and

169 cilia-related genes during spermatogenesis. These findings suggest that the genes
170 identified in our study provide an excellent resource for candidates with novel ciliary or
171 spermatogenesis-related functions, and the newly identified testes-specific protein
172 TULP2(Oyama et al., 2022; Zheng et al., 2021) was selected for validation. We observed
173 that *TULP2* KO male mice were sterile due to malformation of sperm flagella (Figure
174 S4). Overall, our results clearly indicate that XAP5L acts as a central transcriptional
175 repressor of ciliogenesis during mouse spermatogenesis.

176 Furthermore, we performed RNA-seq analysis using P16 testes samples from WT and
177 *XAP5* cKO mice to explore the underlying mechanism of XAP5-mediated germ cell loss.
178 Differential expression analysis identified 554 upregulated and 1587 downregulated
179 genes in *XAP5* cKO sperm (Figure S5A). We observed that the downregulated genes in
180 *XAP5* cKO males were involved in cilium assembly or functions (Figure 4D and Figures
181 S5B-D). Strikingly, many of these downregulated genes were upregulated in *XAP5L* KO
182 sperm, including the key ciliogenesis regulators FOXJ1 and RFX families (Figures 4E, F,
183 Figure S5E and Table S1). In addition, meiosis initiation marker STRA8(Anderson et al.,
184 2008; Ferder et al., 2019), meiosis-specific genes SPO11(Romanienko & Camerini-
185 Otero, 2000) and DMC1(Bishop, Park, Xu, & Kleckner, 1992), key transcription
186 regulators of spermiogenesis RFX2(Kistler et al., 2015; Wu et al., 2016), SOX30(D.
187 Zhang et al., 2018) and CREM(Blendy, Kaestner, Weinbauer, Nieschlag, & Schutz, 1996;
188 Nantel et al., 1996) were also downregulated in *XAP5* cKO mice (Figures 4E and S5F),
189 consistent with the aforementioned result that loss of XAP5 induced spermatogenesis

190 arrest in meiotic stage. Considering the evolutionary conservation of XAP5/XAP5L
191 protein across different species and the expression patterns of XAP5, XAP5L, FOXJ1
192 and RFX factors during spermatogenesis (Figures 1C and S6), these results suggest that
193 XAP5 and XAP5L have antagonistic effects, and they may function upstream of the
194 transcription factor families, including FOXJ1 and RFX factors, to coordinate the
195 ciliogenesis during spermatogenesis (Figure 4G).
196

197 **Discussion**

198 Cilia and flagella are ancient organelles present in the last eukaryotic common ancestor
199 (LECA)(Mitchell, 2017). Cilia assembly and maintenance are under strict transcriptional
200 regulation in both unicellular and multicellular organisms(Choksi et al., 2014; Collins et
201 al., 2021; Lewis & Stracker, 2021; Thomas et al., 2010). Despite cilia and flagella having
202 an ancient origin, the evolutionary history of ciliary gene regulation has remained an
203 unsolved problem. The main reason is that the master ciliary transcription factors found
204 in multicellular organisms, including FOXJ1 and RFXs, are absent from unicellular
205 organisms(Choksi et al., 2014; Collins et al., 2021; Lewis & Stracker, 2021; Thomas et
206 al., 2010). Previously, we showed that an ancient transcription factor, XAP5, was
207 required for flagella assembly in the unicellular green algae *Chlamydomonas*(Li et al.,
208 2018). XAP5 proteins are evolutionarily conserved across diverse organisms(Li et al.,
209 2018; Martin-Tryon & Harmer, 2008), which offers the possibility to investigate the
210 conservation of the role of XAP5 in multicellular organisms. In the present study, we

211 report that XAP5 positively regulates transcriptional network of ciliary genes by
212 activating the key regulators including FOXJ1 and RFXs during spermatogenesis.

213 Cilia are dynamic organelles, and the expression profile of ciliary genes is dynamic
214 during the cell cycle and under certain physiological conditions(Eggenschwiler &
215 Anderson, 2007; Kasahara & Inagaki, 2021; Santos & Reiter, 2008). Cells have
216 developed regulatory mechanisms to generate functional cilia in a temporal and spatial
217 manner(Choksi et al., 2014; Collins et al., 2021; Lewis & Stracker, 2021; Thomas et al.,
218 2010). However, how ciliary transcription factors determine temporal and spatial ciliary
219 transcriptional programs is poorly understood. Sperm flagellar assembly is likewise
220 tightly regulated during a highly complex temporal process named
221 spermatogenesis(Holstein, Schulze, & Davidoff, 2003; Thomas et al., 2010). Several key
222 transcriptional regulators of spermatogenesis, such as FOXJ1 and RFX2, have been
223 identified(Chen, Knowles, Hebert, & Hackett, 1998; Kistler et al., 2015; Wu et al., 2016).
224 The flagellar formation of FOXJ1-null sperm is severely impaired, and the FOXJ1 target
225 genes are required for sperm motility(Beckers et al., 2020; Chen et al., 1998; Weidemann
226 et al., 2016). *RFX2* KO mice are completely sterile and RFX2 regulates the expression of
227 ciliary genes during spermiogenesis(Kistler et al., 2015; Wu et al., 2016). Ciliary
228 transcription factors (FOXJ1 and RFX2) are dynamically regulated during
229 spermatogenesis(Jung et al., 2019). Intriguingly, our results show that XAP5 and XAP5L
230 are two conserved pairs of antagonistic transcription factors that regulate these key
231 transcriptional regulators required for spermatogenesis.

232 By using Western blot analysis, we found that XAP5 was ubiquitously expressed in all
233 tissues examined, whereas XAP5L expression was restricted to the testes (Fig. 1a).
234 Interestingly, previous research found that XAP5L was widely expressed in normal tissue
235 via using TCGA expression data(Thompson et al., 2021). Moreover, loss of
236 XAP5/XAP5L perturbs transcriptional programs in cancer cells. At present, as shown by
237 the recent data, we cannot rule out the possibility that XAP5L is dynamically expressed
238 in other tissues during development. Although XAP5 and XAP5L are highly expressed in
239 testes and critical for spermatogenesis, they are not present in mature sperm (Extended
240 Data Fig. 1). Thus, XAP5/XAP5L are not needed for sperm maintenance. Given the
241 dynamic expression of XAP5/XAP5L during spermatogenesis, it will be interesting to
242 identify the key signaling factors that regulate the timely and spatial expression of XAP5
243 and XAP5L.

244 A role for XAP5 in human brain development is suggested by the association of X-
245 linked intellectual disability (XLID) with rare *XAP5* missense variants(Lee et al., 2020).
246 However, how defects in XAP5 lead to XLID syndrome is unknown. Although there is as
247 yet no evidence that XAP5 regulates ciliogenesis in any system besides *Chlamydomonas*
248 and mice, the function in cilia could help clarify the unexplained role of *XAP5* mutations
249 in causing XLID. The possibility that XAP5 could be a ciliary transcription factor in
250 humans would add XLID to the growing list of the second-order ciliopathies.

251

252

Materials and Methods

Mice

C57BL/6J strains (from Vital River Laboratories, Beijing, China) and *Stra8-GFPCre* knockin mice (from Cyagen Biosciences) were used. Floxed-*XAP5* mice, *XAP5L* and *TULP2* knockout mice were generated on the C57BL/6J background using the CRISPR/Cas9 system. The sgRNA sequences used to target *XAP5*, *XAP5L* and *TULP2* were as follows: *XAP5L*, sgRNA1-GGC TAC CAG AAA CAG GGA CT, sgRNA2-GGG AGT AAG GTC CCC AAA CT; *XAP5*, sgRNA3-CTA CAG GGC ACT TAT TAA TA, sgRNA4-ATA GTA ATT CCC CCG TGC TT; *TULP2*, sgRNA5-TGA CTA ATT AGG CCC GAG AG, sgRNA6-GGT TCT TAG AGA GTC AAC GT. Experimental protocols were approved by the ethics committees of Jianghan University. Mice were maintained in a pathogen-free environment with a room temperature of 23 ± 2 °C under a humidity level of 30-70%. The light was maintained on a 12-hour day/night cycle.

Genome PCR

Mouse genomic DNA was isolated from the tail tip using One Step Mouse Genotyping Kit (Vazyme, PD101), and subjected to PCR with 2 × Taq Plus Master Mix (Vazyme, P212) following the manufacturer's instructions. The PCR products were separated by 2% agarose gel electrophoresis. The primers used are listed in Table S2.

RNA isolation and real-time PCR

Total RNA was isolated using the TRIzol reagent (Invitrogen, 15596018) and then converted to cDNA with HiScript II 1st Strand cDNA Synthesis Kit (Vazyme, R212) following the manufacturer's instructions. Real-time PCR was conducted using ChamQ SYBR qPCR Master Mix (Vazyme, Q311) on an ABI StepOnePlus real-time PCR system (Applied Biosystems). Expression values were normalized using the ΔΔCt method with *Gapdh* as the internal control. The primer sequences are indicated in Table S2.

Western blot analysis

Cell lysates from mouse tissues were prepared in RIPA buffer (Beyotime, P0013B) containing Protease Inhibitor Cocktail (Roche, 11873580001) and 1mM PMSF. Subcellular lysates of testicular nuclear and cytoplasmic fractions were prepared using Nuclear and Cytoplasmic Protein Extraction Kit (Beyotime, P0027) following the manufacturer's instructions. The protein lysates were subjected to standard immunoblotting analysis. Antibodies used were as follows: anti-β-actin (ABclonal, AC026), anti-XAP5 (Prospertech, HU-412003), anti-XAP5 (Sigma, HPA003585), anti-XAP5L (Prospertech, Hu-412001), anti-LMNB (Proteintech, 66095-1-Ig), anti-GAPDH (ABclonal, AC002), anti-FOXJ1 (D360355, Sangon Biotech), anti-RFX2 (K110716P, Solarbio) and anti-TULP2 (Prospertech, Hu-412002).

Immunofluorescence

Mouse testis were fixed in 4% paraformaldehyde in PBS at 4 °C overnight, dehydrated in gradient ethanol, embedded in paraffin, and sectioned into 5 μm slices. After deparaffinization and rehydration, testis sections were boiled in 1 mM EDTA, pH 8.0 for 15 min using a microwave oven for antigen retrieval, followed by cooling to room temperature. The primary antibodies, including anti-XAP5 (Prospertech, HU-412003, 1:250 dilution), anti-XAP5 (Sigma, HPA003585, 1:250 dilution), anti-XAP5L (Prospertech, Hu-412001, 1:250 dilution), anti-lectin PNA, Alexa Fluor 488 Conjugate (ThermoFisher, L21409, 1:250 dilution), and anti-TULP2 (Prospertech, Hu-412002, 1:250 dilution), were then incubated at 4 °C overnight. Subsequently, the sections were incubated with the secondary antibody donkey anti-rabbit Alexa Fluor Plus 488 (Invitrogen, A32790, 1:500 dilution) for 1 hour and DAPI for 5 minutes at room temperature. Images were collected using a Zeiss Axio Vert A1 microscope.

Histological analysis

Testes and epididymides were fixed in Bouin's solution (sigma, HT10132) overnight at 4 °C, embedded in paraffin and sectioned into 5 μm slices. The sections were then subjected to H&E staining using standard procedures and observed under a Zeiss Axio Vert A1 microscope.

Assessment of sperm motility and morphology

Cauda epididymides were collected from male mice and dissected in 37°C pre-warmed human tubal fluid (HTF) culture medium (EasyCheck, M1130), followed by incubation at 37°C for 15 min to release the sperm. To assess sperm motility, the sperm suspension was observed and recorded under a Leica total internal reflection fluorescence microscope. Motility was defined as any movement of the sperm flagellum during a 10-second observation cycle. After immobilization with 1% paraformaldehyde, sperm morphology was observed by H&E staining using standard procedures. Images were captured using a Zeiss Axio Vert A1 microscope equipped with a ×100 oil immersion objective. Sperm without staining were also used to assess sperm morphology. For ultrastructural observation, sperm samples were fixed in 3% glutaraldehyde in 0.1M sodium phosphate buffer (pH7.4), and post-fixed with 1% (wt/vol) OsO_4. After dehydration, the samples were placed in propylene oxide and embedded in a mixture of Epon 812 and Araldite. Ultrathin sections obtained by a Leica EM UC7 ultramicrotome were stained with uranyl acetate and lead citrate, then analyzed using a HT7700 TEM (Hitachi).

Fertility test

Each of the adult male mice was mated with two females for 2 months. All the mice used were aged 6-8 weeks. Vaginal plugs were checked every morning, and the number of newborn pups was counted.

Chromosome spreads and immunofluorescence

Testicular chromosome spreads were prepared and immunolabeled as described(Reinholdt, Ashley, Schimenti, & Shima, 2004). The primary antibodies used were as follows: anti-γ H2AX (Millipore, 05-636, 1:300 dilution), anti-SYCP3 (Proteintech, 23024-1-AP, 1:300 dilution). Secondary antibodies used were Alexa Dye (AlexaFluor Plus 488/594) conjugates (ThermoFisher) at 1:500 dilutions. Images were collected with a Zeiss Axio Vert A1 microscope.

RNA-seq analysis

The mature sperm samples from P56 mice and testis samples from P16 mice were washed three time in 1× PBS after harvest. Total RNA was extracted from the samples using the TRIzol reagent (Invitrogen) and purified with the NEBNext Poly(A) mRNA Magnetic Isolation Module (NEB, E7490). The quality of the RNA samples was examined using the Agilent 2100 Bioanalyzer system (Agilent Technologies). Qualified RNA samples were subjected to sequencing library construction using the NEBNext Ultra II RNA Library Prep Kit for Illumina (NEB, E7775). Paired-end (2 × 150 bp) sequencing was carried out on the Illumina NovaSeq6000 platform. The sequencing reads were mapped to the Mus musculus reference genome (GRCm38/mm10) using HISAT2 v2.1.0(Kim, Langmead, & Salzberg, 2015), and StringTie v1.3.3b(Pertea et al., 2015) was applied to assemble the mapped reads. Fragments Per Kilobase of transcript per Million fragments mapped (FPKM) was used to measure the expression level of a gene.

Differential expression analysis was processed by DESeq2 v1.12.4(Subramanian et al., 2005), and the significant differentially expressed genes were identified with a fold change >2. Gene Ontology analysis was performed using the DAVID database.

Statistical analysis

Statistical analyses were conducted using GraphPad Prism 8.0.2 software. All data were presented as mean ± SEM. Values of $P < 0.05$ were considered statistically significant. Statistical significance between two groups was calculated using an unpaired, parametric, two-sided student's t test.

Data availability

All relevant data for RNA sequencing have been deposited in the Gene Expression Omnibus database under accession code GSE236388. The authors declare that the data supporting the findings of this study are available within the article and its supplementary materials or from the corresponding author upon reasonable request.

Acknowledgements

This work was supported by the National Key R&D Program of China (grant number: 2020YFA0907400), the National Natural Science Foundation of China (grant number: 32170702 and 82000828) and the Major Special Funding Program for First-class

Discipline Construction of Jianghan University (grant number: 2023XKZ021). We thank Yuan He (Research Center for Medicine and Structural Biology, Wuhan University, China) for the assistance during the experimental design of the transmission electron microscope analysis.

Author Contributions

W.W., J.X., X.Z. and Z.H. designed research; W.W., J.X., X.Z., H.L., H.J., C.X. and X.Z. performed research; W.W. and Z.H. contributed new reagents/analytic tools; W.W., J.X., X.Z. and Z.H. analyzed data; and W.W. and Z.H. wrote the paper.

Competing interests

The authors declare no competing interests.

Additional files

Table S1

The lists of differential expression genes & ciliogenesis-related genes.

Table S2

The lists of primers used in the Genome PCR and real-time PCR.

Video S1

Representative video of living sperm cells from WT mouse.

Video S2

398 Representative video of living sperm cells from *XAP5L* KO mouse.

399

400 **References**

401 Anderson, E. L., Baltus, A. E., Roepers-Gajadien, H. L., Hassold, T. J., de Rooij, D. G., van Pelt,
402 A. M., & Page, D. C. (2008). Stra8 and its inducer, retinoic acid, regulate meiotic initiation
403 in both spermatogenesis and oogenesis in mice. *Proc Natl Acad Sci U S A, 105*(39),
404 14976-14980. doi:10.1073/pnas.0807297105

405 Beckers, A., Adis, C., Schuster-Gossler, K., Tveriakhina, L., Ott, T., Fuhl, F., . . . Gossler, A.
406 (2020). The FOXJ1 target Cfap206 is required for sperm motility, mucociliary clearance of
407 the airways and brain development. *Development*. doi:10.1242/dev.188052

408 Bishop, D. K., Park, D., Xu, L., & Kleckner, N. (1992). DMC1: a meiosis-specific yeast homolog of
409 E. coli recA required for recombination, synaptonemal complex formation, and cell cycle
410 progression. *Cell, 69*(3), 439-456. doi:10.1016/0092-8674(92)90446-j

411 Blendy, J. A., Kaestner, K. H., Weinbauer, G. F., Nieschlag, E., & Schutz, G. (1996). Severe
412 impairment of spermatogenesis in mice lacking the CREM gene. *Nature, 380*(6570), 162-
413 165. doi:10.1038/380162a0

414 Chen, J., Knowles, H. J., Hebert, J. L., & Hackett, B. P. (1998). Mutation of the mouse hepatocyte
415 nuclear factor/forkhead homologue 4 gene results in an absence of cilia and random left-
416 right asymmetry. *J Clin Invest, 102*(6), 1077-1082. doi:10.1172/JCI4786

417 Choksi, S. P., Lauter, G., Swoboda, P., & Roy, S. (2014). Switching on cilia: transcriptional

418 networks regulating ciliogenesis. *Development, 141*(7), 1427-1441.
419 doi:10.1242/dev.074666
420 Chu, J. S., Baillie, D. L., & Chen, N. (2010). Convergent evolution of RFX transcription factors
421 and ciliary genes predated the origin of metazoans. *BMC Evol Biol, 10*, 130.
422 doi:10.1186/1471-2148-10-130
423 Collins, C., Ventrella, R., & Mitchell, B. J. (2021). Building a ciliated epithelium: Transcriptional
424 regulation and radial intercalation of multiciliated cells. *Curr Top Dev Biol, 145*, 3-39.
425 doi:10.1016/bs.ctdb.2020.08.001
426 Derderian, C., Canales, G. I., & Reiter, J. F. (2023). Seriously cilia: A tiny organelle illuminates
427 evolution, disease, and intercellular communication. *Dev Cell, 58*(15), 1333-1349.
428 doi:10.1016/j.devcel.2023.06.013
429 Eggenschwiler, J. T., & Anderson, K. V. (2007). Cilia and developmental signaling. *Annu Rev Cell*
430 *Dev Biol, 23*, 345-373. doi:10.1146/annurev.cellbio.23.090506.123249
431 Ferder, I. C., Fung, L., Ohguchi, Y., Zhang, X., Lassen, K. G., Capen, D., . . . Wang, N. (2019).
432 Meiotic gatekeeper STRA8 suppresses autophagy by repressing Nr1d1 expression
433 during spermatogenesis in mice. *PLoS Genet, 15*(5), e1008084.
434 doi:10.1371/journal.pgen.1008084
435 Goetz, S. C., & Anderson, K. V. (2010). The primary cilium: a signalling centre during vertebrate
436 development. *Nat Rev Genet, 11*(5), 331-344. doi:10.1038/nrg2774
437 Holstein, A.-F., Schulze, W., & Davidoff, M. (2003). Understanding spermatogenesis is a

438 prerequisite for treatment. *Reproductive Biology and Endocrinology, 1*(1).
439 doi:10.1186/1477-7827-1-107
440 Ishikawa, H., & Marshall, W. F. (2011). Ciliogenesis: building the cell's antenna. *Nat Rev Mol Cell*
441 *Biol, 12*(4), 222-234. doi:10.1038/nrm3085
442 Jung, M., Wells, D., Rusch, J., Ahmad, S., Marchini, J., Myers, S. R., & Conrad, D. F. (2019).
443 Unified single-cell analysis of testis gene regulation and pathology in five mouse strains.
444 *Elife, 8*. doi:10.7554/eLife.43966
445 Kasahara, K., & Inagaki, M. (2021). Primary ciliary signaling: links with the cell cycle. *Trends Cell*
446 *Biol, 31*(12), 954-964. doi:10.1016/j.tcb.2021.07.009
447 Kim, D., Langmead, B., & Salzberg, S. L. (2015). HISAT: a fast spliced aligner with low memory
448 requirements. *Nat Methods, 12*(4), 357-360. doi:10.1038/nmeth.3317
449 Kistler, W. S., Baas, D., Lemeille, S., Paschaki, M., Seguin-Estevez, Q., Barras, E., . . . Reith, W.
450 (2015). RFX2 Is a Major Transcriptional Regulator of Spermiogenesis. *PLoS Genet, 11*(7),
451 e1005368. doi:10.1371/journal.pgen.1005368
452 Lee, Y.-R., Khan, K., Armfield-Uhas, K., Srikanth, S., Thompson, N. A., Pardo, M., . . . Schwartz,
453 C. E. (2020). Mutations in FAM50A suggest that Armfield XLID syndrome is a
454 spliceosomopathy. *Nature Communications, 11*(1). doi:10.1038/s41467-020-17452-6
455 Lewis, M., & Stracker, T. H. (2021). Transcriptional regulation of multiciliated cell differentiation.
456 *Semin Cell Dev Biol, 110*, 51-60. doi:10.1016/j.semcdb.2020.04.007
457 Li, L., Tian, G., Peng, H., Meng, D., Wang, L., Hu, X., . . . Hu, Z. (2018). New class of

458 transcription factors controls flagellar assembly by recruiting RNA polymerase II in
459 Chlamydomonas. *Proc Natl Acad Sci U S A, 115*(17), 4435-4440.
460 doi:10.1073/pnas.1719206115
461 Lin, Z., Hsu, P. J., Xing, X., Fang, J., Lu, Z., Zou, Q., . . . Tong, M. H. (2017). Mettl3-/Mettl14-
462 mediated mRNA N(6)-methyladenosine modulates murine spermatogenesis. *Cell Res,*
463 *27*(10), 1216-1230. doi:10.1038/cr.2017.117
464 Lovera, M., & Lüders, J. (2021). The ciliary impact of nonciliary gene mutations. *Trends Cell Biol,*
465 *31*(11), 876-887. doi:10.1016/j.tcb.2021.06.001
466 Martianov, I., Fimia, G. M., Dierich, A., Parvinen, M., Sassone-Corsi, P., & Davidson, I. (2001).
467 Late arrest of spermiogenesis and germ cell apoptosis in mice lacking the TBP-like
468 TLF/TRF2 gene. *Mol Cell, 7*(3), 509-515. doi:10.1016/s1097-2765(01)00198-8
469 Martin-Tryon, E. L., & Harmer, S. L. (2008). XAP5 CIRCADIAN TIMEKEEPER coordinates light
470 signals for proper timing of photomorphogenesis and the circadian clock in Arabidopsis.
471 *Plant Cell, 20*(5), 1244-1259. doi:10.1105/tpc.107.056655
472 Mazzarella, R., Pengue, G., Yoon, J., Jones, J., & Schlessinger, D. (1997). Differential expression
473 of XAP5, a candidate disease gene. *Genomics, 45*(1), 216-219.
474 doi:10.1006/geno.1997.4912
475 Mitchell, D. R. (2017). Evolution of Cilia. *Cold Spring Harb Perspect Biol, 9*(1).
476 doi:10.1101/cshperspect.a028290
477 Nachury, M. V., & Mick, D. U. (2019). Establishing and regulating the composition of cilia for

478 signal transduction. *Nat Rev Mol Cell Biol*. doi:10.1038/s41580-019-0116-4

479 Nantel, F., Monaco, L., Foulkes, N. S., Masquilier, D., LeMeur, M., Henriksen, K., . . . Sassone-
480 Corsi, P. (1996). Spermiogenesis deficiency and germ-cell apoptosis in CREM-mutant
481 mice. *Nature, 380*(6570), 159-162. doi:10.1038/380159a0

482 Nemajerova, A., Kramer, D., Siller, S. S., Herr, C., Shomroni, O., Pena, T., . . . Lize, M. (2016).
483 TAp73 is a central transcriptional regulator of airway multiciliogenesis. *Genes Dev,*
484 *30*(11), 1300-1312. doi:10.1101/gad.279836.116

485 Oyama, Y., Miyata, H., Shimada, K., Larasati, T., Fujihara, Y., & Ikawa, M. (2022). TULP2
486 deletion mice exhibit abnormal outer dense fiber structure and male infertility. *Reprod*
487 *Med Biol, 21*(1), e12467. doi:10.1002/rmb2.12467

488 Pertea, M., Pertea, G. M., Antonescu, C. M., Chang, T.-C., Mendell, J. T., & Salzberg, S. L.
489 (2015). StringTie enables improved reconstruction of a transcriptome from RNA-seq
490 reads. *Nature Biotechnology, 33*(3), 290-295. doi:10.1038/nbt.3122

491 Piasecki, B. P., Burghoorn, J., & Swoboda, P. (2010). Regulatory Factor X (RFX)-mediated
492 transcriptional rewiring of ciliary genes in animals. *Proc Natl Acad Sci U S A, 107*(29),
493 12969-12974. doi:10.1073/pnas.0914241107

494 Qu, W., Yuan, S., Quan, C., Huang, Q., Zhou, Q., Yap, Y., . . . Zhang, Z. (2020). The essential
495 role of intraflagellar transport protein IFT81 in male mice spermiogenesis and fertility. *Am*
496 *J Physiol Cell Physiol, 318*(6), C1092-C1106. doi:10.1152/ajpcell.00450.2019

497 Reinholdt, L., Ashley, T., Schimenti, J., & Shima, N. (2004). Forward genetic screens for meiotic

498 and mitotic recombination-defective mutants in mice. *Methods Mol Biol, 262*, 87-107.
499 doi:10.1385/1-59259-761-0:087
500 Reiter, J. F., & Leroux, M. R. (2017). Genes and molecular pathways underpinning ciliopathies.
501 *Nat Rev Mol Cell Biol, 18*(9), 533-547. doi:10.1038/nrm.2017.60
502 Romanienko, P. J., & Camerini-Otero, R. D. (2000). The mouse Spo11 gene is required for
503 meiotic chromosome synapsis. *Mol Cell, 6*(5), 975-987. doi:10.1016/s1097-
504 2765(00)00097-6
505 Santos, N., & Reiter, J. F. (2008). Building it up and taking it down: the regulation of vertebrate
506 ciliogenesis. *Dev Dyn, 237*(8), 1972-1981. doi:10.1002/dvdy.21540
507 Schartl, M., Schories, S., Wakamatsu, Y., Nagao, Y., Hashimoto, H., Bertin, C., . . . Herpin, A.
508 (2018). Sox5 is involved in germ-cell regulation and sex determination in medaka
509 following co-option of nested transposable elements. *BMC Biol, 16*(1), 16.
510 doi:10.1186/s12915-018-0485-8
511 Sedlacek, Z., Munstermann, E., Dhorne-Pollet, S., Otto, C., Bock, D., Schutz, G., & Poustka, A.
512 (1999). Human and mouse XAP-5 and XAP-5-like (X5L) genes: identification of an
513 ancient functional retroposon differentially expressed in testis. *Genomics, 61*(2), 125-132.
514 doi:10.1006/geno.1999.5931
515 Singla, V., & Reiter, J. F. (2006). The primary cilium as the cell's antenna: signaling at a sensory
516 organelle. *Science, 313*(5787), 629-633. doi:10.1126/science.1124534
517 Stubbs, J. L., Oishi, I., Izpisua Belmonte, J. C., & Kintner, C. (2008). The forkhead protein Foxj1

518 specifies node-like cilia in Xenopus and zebrafish embryos. *Nat Genet, 40*(12), 1454-
519 1460. doi:10.1038/ng.267
520 Subramanian, A., Tamayo, P., Mootha, V. K., Mukherjee, S., Ebert, B. L., Gillette, M. A., . . .
521 Mesirov, J. P. (2005). Gene set enrichment analysis: A knowledge-based approach for
522 interpreting genome-wide expression profiles. *Proceedings of the National Academy of*
523 *Sciences, 102*(43), 15545-15550. doi:10.1073/pnas.0506580102
524 Swoboda, P., Adler, H. T., & Thomas, J. H. (2000). The RFX-type transcription factor DAF-19
525 regulates sensory neuron cilium formation in C. elegans. *Mol Cell, 5*(3), 411-421.
526 doi:10.1016/s1097-2765(00)80436-0
527 Thomas, J., Morle, L., Soulavie, F., Laurencon, A., Sagnol, S., & Durand, B. (2010).
528 Transcriptional control of genes involved in ciliogenesis: a first step in making cilia. *Biol*
529 *Cell, 102*(9), 499-513. doi:10.1042/BC20100035
530 Thompson, N. A., Ranzani, M., van der Weyden, L., Iyer, V., Offord, V., Droop, A., . . . Adams, D.
531 J. (2021). Combinatorial CRISPR screen identifies fitness effects of gene paralogues.
532 *Nature Communications, 12*(1). doi:10.1038/s41467-021-21478-9
533 Vij, S., Rink, J. C., Ho, H. K., Babu, D., Eitel, M., Narasimhan, V., . . . Roy, S. (2012).
534 Evolutionarily ancient association of the FoxJ1 transcription factor with the motile
535 ciliogenic program. *PLoS Genet, 8*(11), e1003019. doi:10.1371/journal.pgen.1003019
536 Weidemann, M., Schuster-Gossler, K., Stauber, M., Wrede, C., Hegermann, J., Ott, T., . . .
537 Gossler, A. (2016). CFAP157 is a murine downstream effector of FOXJ1 that is

538 specifically required for flagellum morphogenesis and sperm motility. *Development, 143*(24), 4736-4748. doi:10.1242/dev.139626

540 Wu, Y., Hu, X., Li, Z., Wang, M., Li, S., Wang, X., . . . Han, C. (2016). Transcription Factor RFX2 Is a Key Regulator of Mouse Spermiogenesis. *Sci Rep, 6*, 20435. doi:10.1038/srep20435

542 Yu, X., Ng, C. P., Habacher, H., & Roy, S. (2008). Foxj1 transcription factors are master regulators of the motile ciliogenic program. *Nat Genet, 40*(12), 1445-1453. doi:10.1038/ng.263

545 Zhang, A., Skaar, D. A., Li, Y., Huang, D., Price, T. M., Murphy, S. K., & Jirtle, R. L. (2011). Novel retrotransposed imprinted locus identified at human 6p25. *Nucleic Acids Res, 39*(13), 5388-5400. doi:10.1093/nar/gkr108

548 Zhang, D., Xie, D., Lin, X., Ma, L., Chen, J., Zhang, D., . . . Han, C. (2018). The transcription factor SOX30 is a key regulator of mouse spermiogenesis. *Development, 145*(11). doi:10.1242/dev.164723

551 Zheng, M., Chen, X., Cui, Y., Li, W., Dai, H., Yue, Q., . . . Zhu, H. (2021). TULP2, a New RNA-Binding Protein, Is Required for Mouse Spermatid Differentiation and Male Fertility. *Front Cell Dev Biol, 9*, 623738. doi:10.3389/fcell.2021.623738

554 Zhou, H., Grubisic, I., Zheng, K., He, Y., Wang, P. J., Kaplan, T., & Tjian, R. (2013). Taf7l cooperates with Trf2 to regulate spermiogenesis. *Proc Natl Acad Sci U S A, 110*(42), 16886-16891. doi:10.1073/pnas.1317034110

557

558 **Figures**

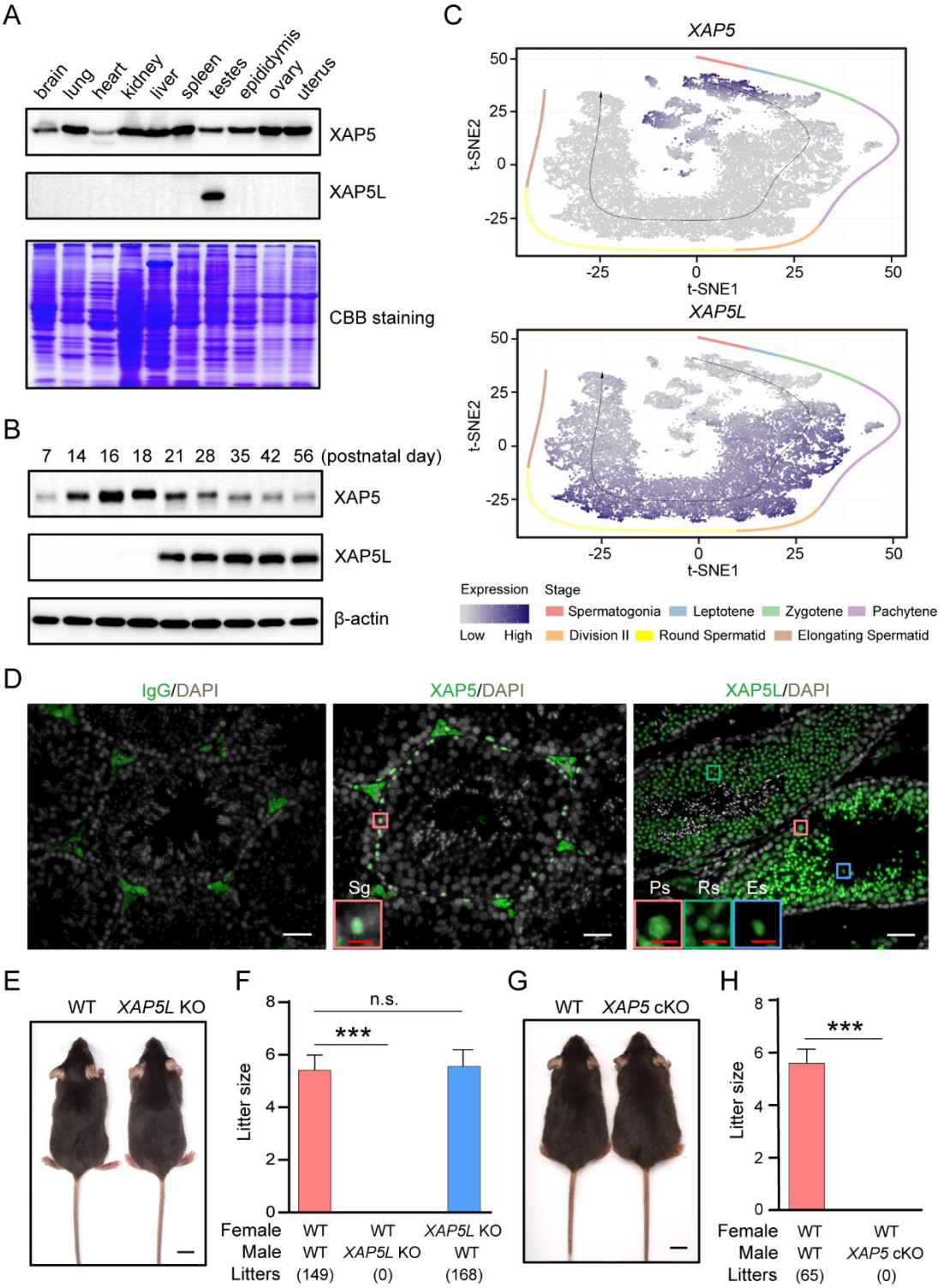

559

560 **Figure 1. Loss of XAP5 and XAP5L proteins results in male mice infertility.**

561 **(A)** Detection of XAP5/XAP5L protein in different tissues of adult mice by Western blot
562 analysis. **(B)** Expression of XAP5/XAP5L protein during postnatal testicular
563 development. β-actin was used as control. **(C)** t-SNE plots displaying *XAP5*/*XAP5L* gene
564 expression levels in individual cell types of mouse testis visualized using published
565 single-cell data(Jung et al., 2019). Black arrow represents the developmental pseudotime
566 corresponding to the developmental ordering of each cell progressing through
567 spermatogenesis. Dot color intensity represents the expression level. Cells from different
568 stages are color-coded. **(D)** Immunofluorescence staining of XAP5/XAP5L in adult WT
569 testis. Representative spermatogonium (Sg), round spermatid (Rs) and elongating
570 spermatid (Es) are indicated. Scale bars: 20 μm (white), 5 μm (red). **(E)** Similar
571 development between WT and *XAP5L* KO mice. Scale bar: 1 cm. **(F)** Average litter size
572 of pups obtained by fertility test. Each male was caged with two females for 2 months, 5
573 males were used for each genotype. ***$P < 0.001$, n.s. stands for not significant. **(G)**
574 Similar appearance of WT and *XAP5* cKO mice. Scale bar: 1 cm. **(H)** Average litter size
575 of pups obtained by fertility test. Each male was caged with two WT females for 2
576 months, 4 males were used for each genotype. ***$P < 0.001$. Error bars depict means ±
577 SEM. All *P*-values were calculated using an unpaired, two-tailed Student's t-test.

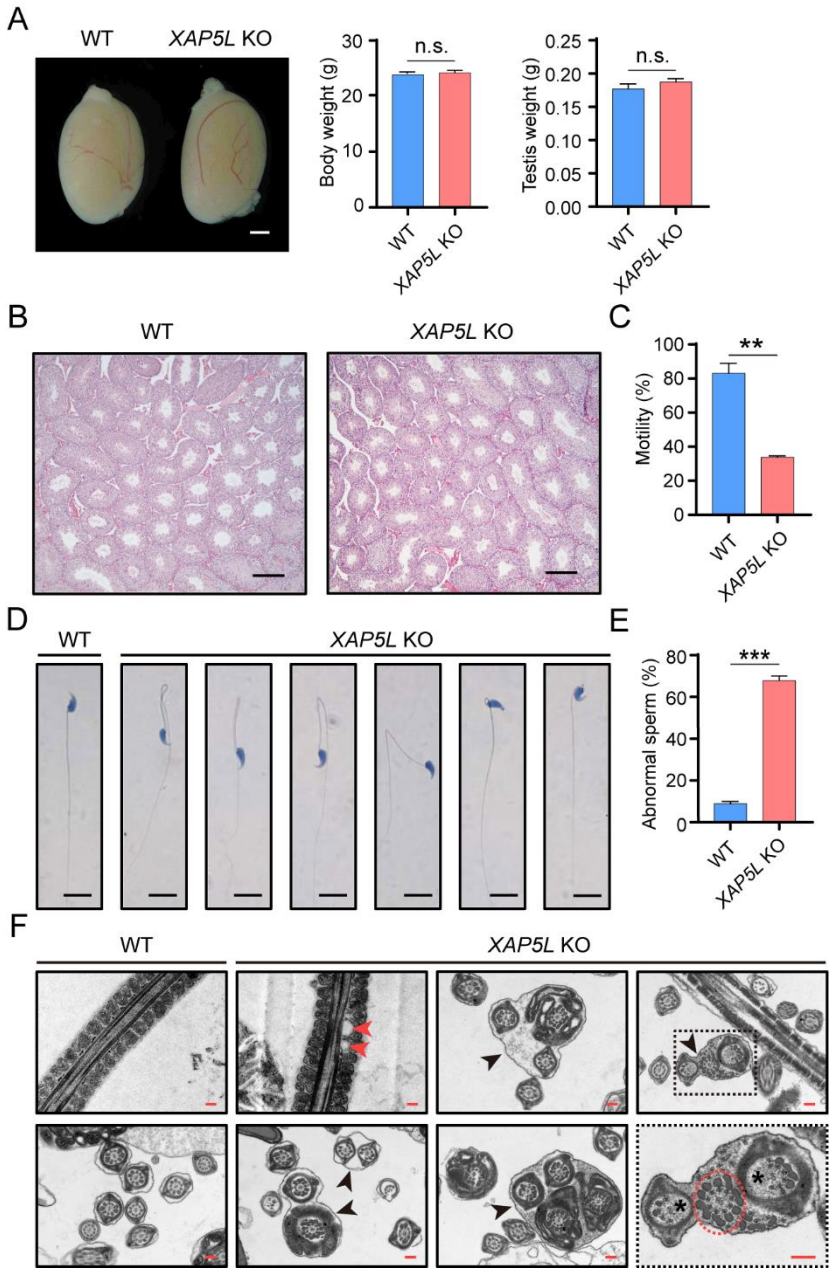

578

579 **Figure 2. XAP5L is required for normal sperm formation.**

580 **(A)** Similar gross testes morphology, body weight and testis weight between WT and

581 *XAP5L* KO mice. Scale bar: 1 mm. n = 6, n.s. stands for not significant. **(B)** H&E

582 staining showing similar histological structure of the testes from WT and *XAP5L* KO

583 mice. Scale bars: 100 μm. **(C)** Significantly reduced sperm total motility of *XAP5L* KO

584 mice. n = 3, **$P < 0.01$. **(D)** H&E staining showing the morphology of sperm in WT and
585 *XAP5L* KO mice. Scale bars: 10 μm. **(E)** Significantly increased abnormal sperm in
586 *XAP5L* KO mice. n = 6, ***$P < 0.001$. **(F)** Electron microscopic analysis displaying
587 ultrastructural defects in *XAP5L* KO sperm flagella, including cytoplasmic vacuoles
588 enveloping mitochondrial sheath (as shown by red arrowheads), a complete lack of
589 mitochondrial sheath (as shown by red dotted circle), two or more cross-sections of the
590 same sperm flagellum enclosed within one cell membrane (as shown by black
591 arrowheads), partially formed outer dense fibers, and the axonemal microtubules (as
592 indicated by asterisks). Scale bars: 2 μm. Error bars depict means ± SEM. All *P*-values
593 were calculated using an unpaired, two-tailed Student's t-test.

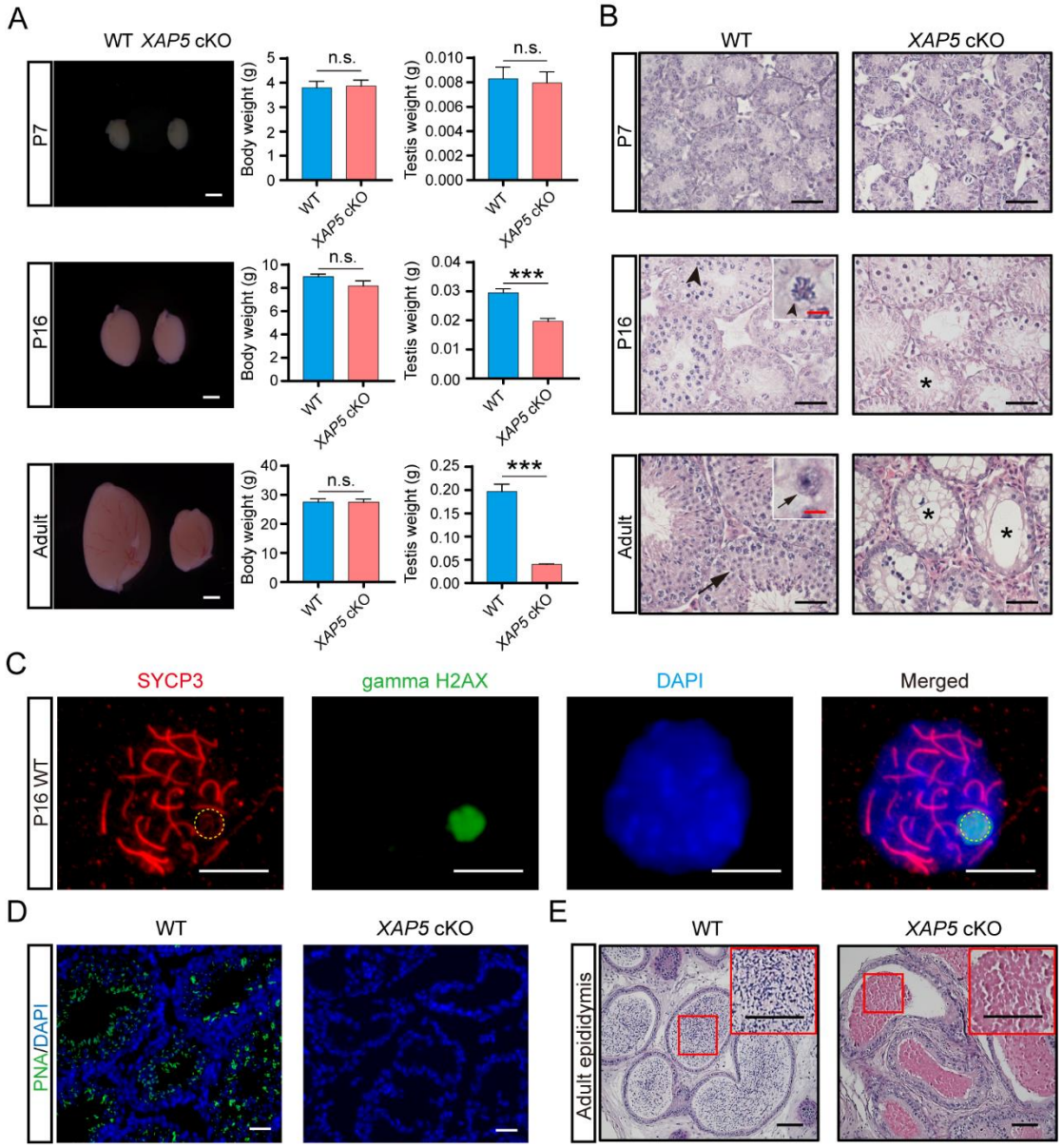

Figure 3. Ablation of XAP5 in germ cells results in arrested spermatogenesis and absence of sperm.

(A) Testes sizes, body weight and testis weight from WT and *XAP5* cKO mice at various ages were evaluated. Similar body weight was observed between WT and *XAP5* cKO mice. No significant difference in size and weight was detected between WT and *XAP5* cKO testes until P16. Scale bars: 1 mm. n = 5, ***$P < 0.001$, n.s. stands for not

601 significant. **(B)** Histology of testes from WT and *XAP5* cKO mice at various ages were
602 evaluated by H&E staining. No pachytene spermatocytes were found, and many
603 vacuolated tubules were observed in *XAP5* cKO testis since P16. Black arrowheads
604 indicate pachytene spermatocytes; black arrows indicate round spermatids. Vacuolated
605 seminiferous tubules are indicated by asterisks. Scale bars: 20 μm (black), 2.5 μm (red).
606 **(C)** Chromosome spreads staining showing pachytene spermatocytes from P16 WT male
607 mouse. Yellow dotted circle indicates the XY body. Scale bars: 10 μm. **(D)**
608 Immunofluorescence staining of PNA in adult testes indicating the absence of spermatids
609 in *XAP5* cKO mice. Scale bars: 20 μm. **(E)** H&E staining of adult epididymis displaying
610 absence of sperm in *XAP5* cKO mice. Scale bars: 50 μm. Error bars depict means ± SEM.
611 All *P*-values were calculated using an unpaired, two-tailed Student's t-test.

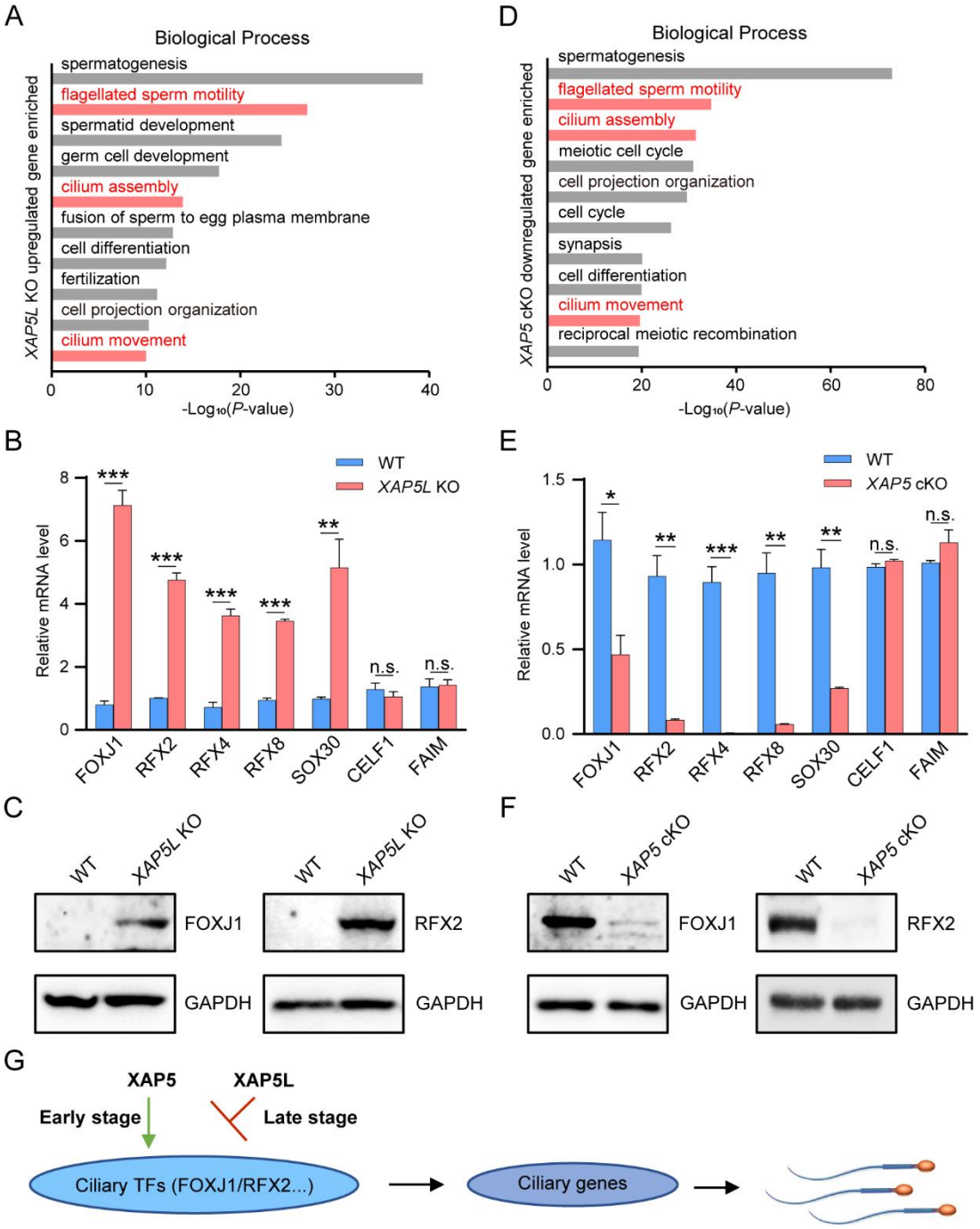

Figure 4. Aberrant ciliogenic and spermatogenic gene expression in *XAP5L* KO and *XAP5* cKO male germ cells.

(A) Gene ontology analysis showing top ten biological process terms significantly enriched among upregulated genes in *XAP5L* KO sperm. **(B)** Real-time PCR validation of

617 genes involved in ciliogenesis and spermatogenesis. n = 3, $^{**}P < 0.01$, $^{***}P < 0.001$, n.s.
618 stands for not significant. **(C)** Detection of FOXJ1 and RFX2 in mature sperm of WT and
619 *XAP5L* KO mice by Western blot analysis. GAPDH was used as a control. **(D)** Gene
620 ontology analysis showing top ten biological process terms significantly enriched among
621 downregulated genes in P16 *XAP5* cKO testes. **(E)** Real-time PCR validation of genes
622 involved in ciliogenesis and spermatogenesis. n = 3, $^{*}P < 0.05$, $^{**}P < 0.01$, $^{***}P < 0.001$,
623 n.s. stands for not significant. **(F)** Detection of FOXJ1 and RFX2 in P16 testes of WT and
624 *XAP5* cKO mice by Western blot analysis. GAPDH was used as a control. **(G)** A model
625 on the involvement of XAP5 and XAP5L in the regulation of ciliogenesis during
626 spermatogenesis. Error bars depict means ± SEM. All *P*-values were calculated using an
627 unpaired, two-tailed Student's t-test.
628
629
630
631
632
633
634
635
636
637

638 **Supplementary Figures**

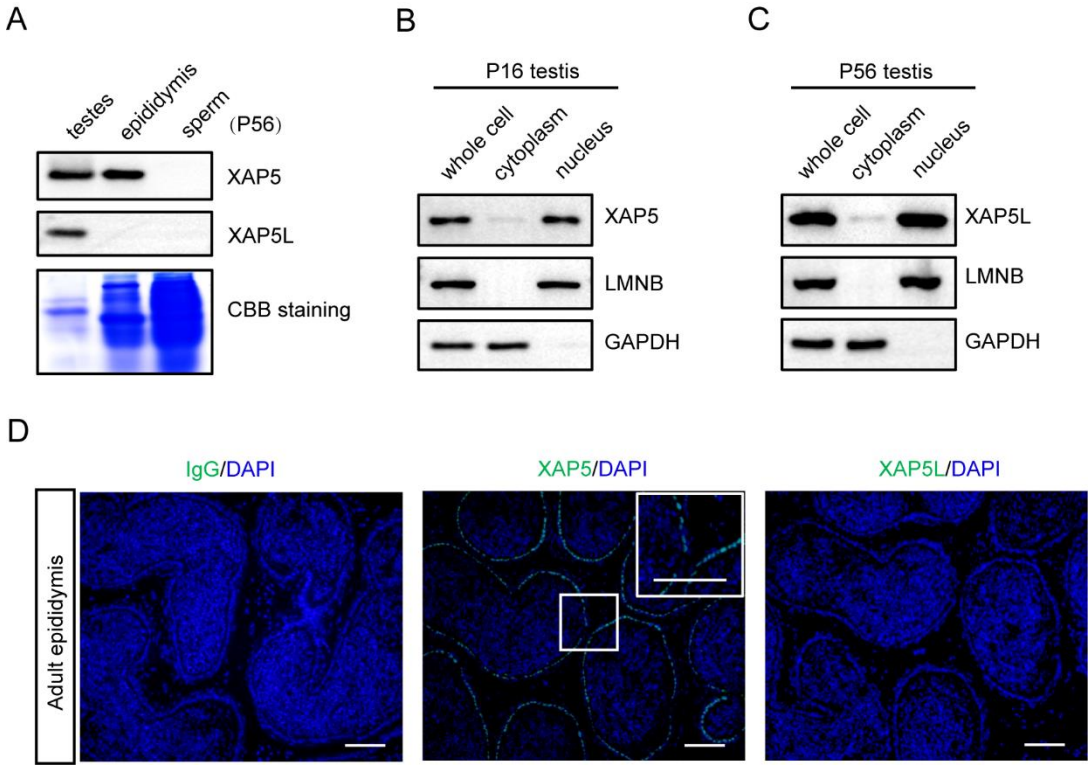

639

640 **Figure S1. Localization of XAP5/XAP5L in testicular cells.**

641 **(A)** Western blot analysis showing no localization of XAP5/XAP5L in mature sperm.
642 Western blot analysis showing the subcellular localization of endogenous XAP5 (**B**) and
643 XAP5L (**C**). LMNB used as a nuclear protein marker, GAPDH used as a cytoplasmic
644 protein marker. **(D)** Immunofluorescence staining of XAP5/XAP5L in adult epididymis.
645 Scale bars: 50 μm.

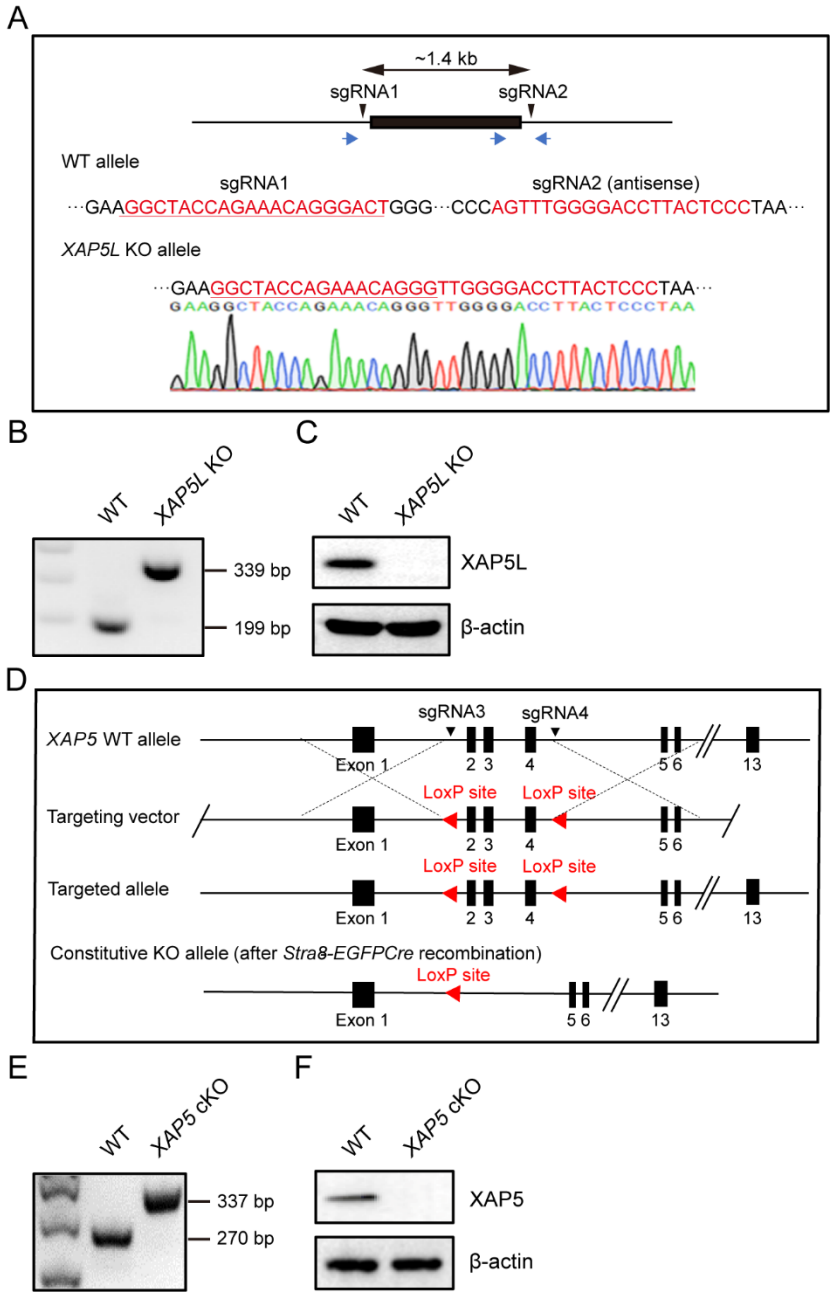

Figure S2. Generation of *XAP5L* KO and *XAP5* cKO mice.

(A) Schematic illustration of the targeting strategy for generating a *XAP5L* knockout mouse line using CRISPR-Cas9 system. Upper panel showing genomic structure of the *XAP5L* gene. The location of two sgRNAs (sgRNA1 and sgRNA2) used and three primers (blue arrows) for genome PCR are indicated. Lower panel displaying nucleotide

652 sequence of WT allele in the vicinity of two sgRNAs (red color) and the corresponding
653 sequence of the *XAP5L* homozygous mutant (KO) allele. The deletion of *XAP5L* gene
654 was verified by Sanger sequencing. **(B)** Genome PCR analysis in WT and *XAP5L* KO
655 mice. **(C)** Detection of XAP5L in adult testes extracts of WT and *XAP5L* KO mice by
656 Western blot analysis. β-actin was used as a control. **(D)** Schematic illustration of the
657 targeting strategy for generating *XAP5* cKO mice. The location of LoxP sites inserted and
658 the primers (blue arrow) used for genome PCR are indicated. **(E)** Genome PCR analysis
659 in WT and *XAP5* cKO mice. **(F)** Detection of XAP5 in testes extracts of WT and *XAP5*
660 cKO mice by Western blot analysis. β-actin was used as a control.

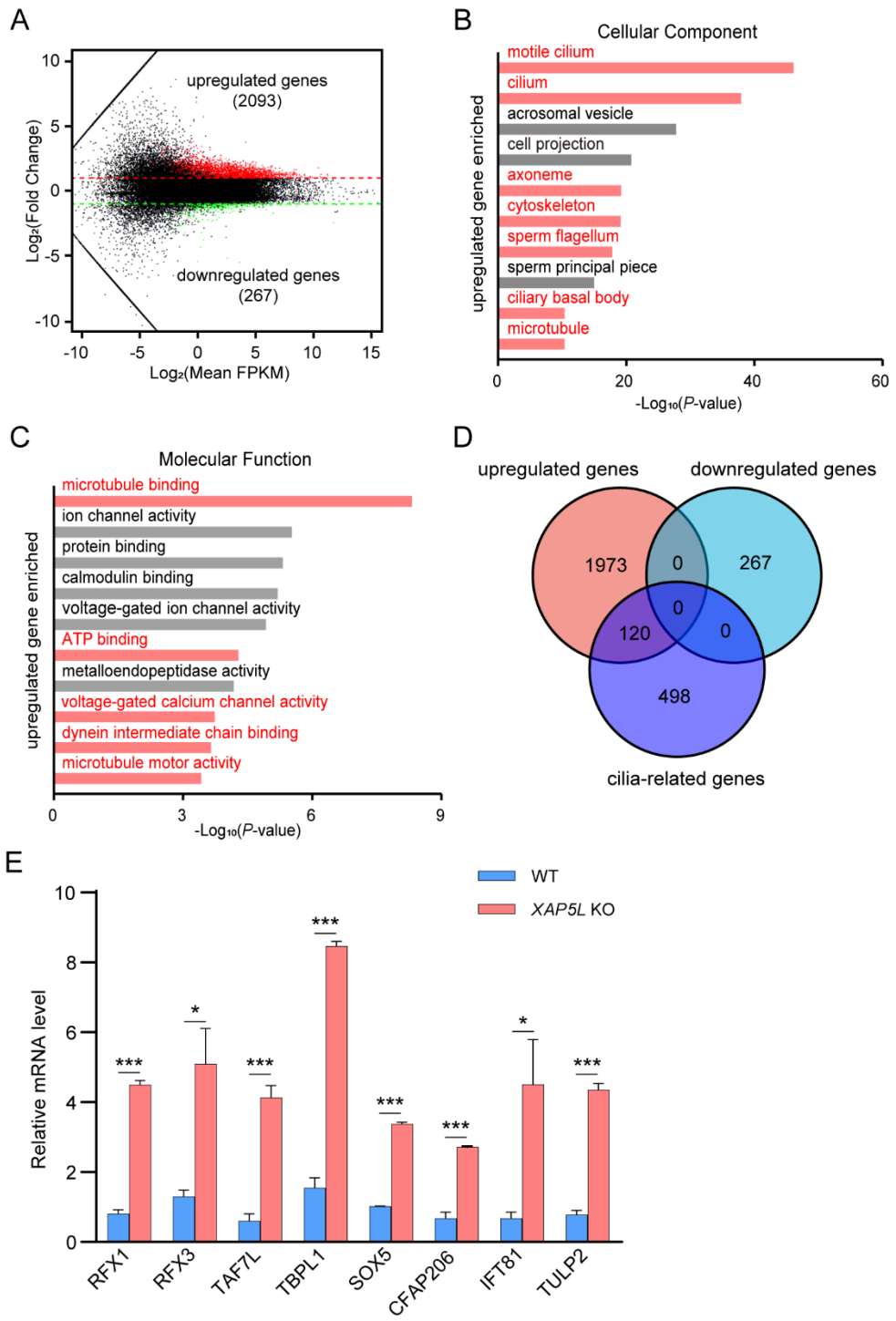

Figure S3. XAP5L-mediated regulation of ciliary gene expression during mouse spermatogenesis.

(A) MA plot showing the numbers of differentially expressed genes in *XAP5L* KO sperm.

665 Gene ontology analysis showing top ten cellular component (**B**) and molecular function
666 (**C**) terms significantly enriched among upregulated genes in *XAP5L* KO sperm. **(D)**
667 Venn diagram representing total genes upregulated/downregulated by at least twofold in
668 *XAP5L* KO sperm and published cilia-related genes(Nemajerova et al., 2016). **(E)** Real-
669 time PCR validation of genes involved in ciliogenesis and spermatogenesis. n = 3, *$P <$
670 0.05, ***$P < 0.001$. Error bars depict means ± SEM. All P-values were calculated using
671 an unpaired, two-tailed Student's t-test.

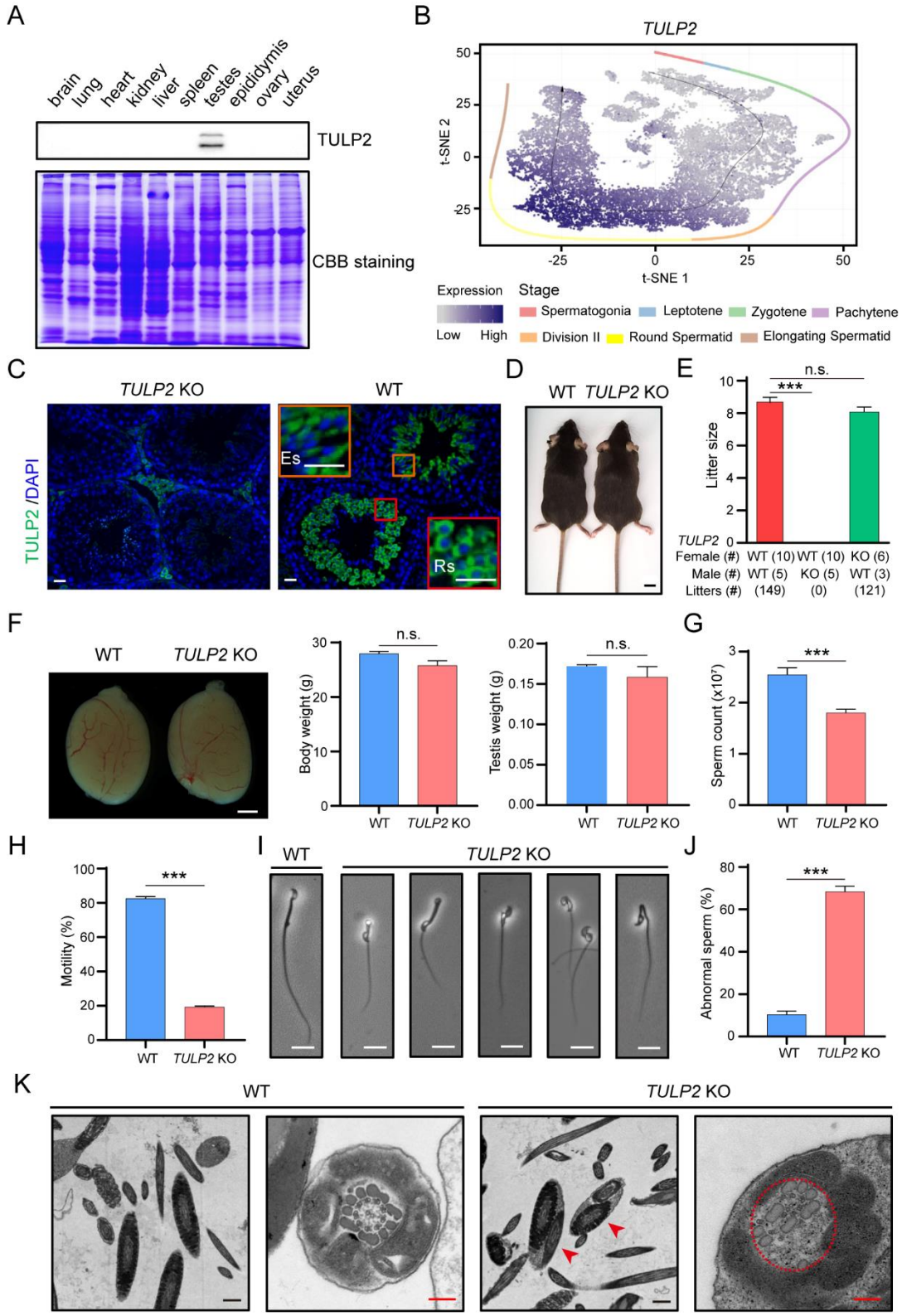

Figure S4. *TULP2* KO male mice were infertile due to malformation of sperm.

(A) Detection of TULP2 protein in different tissues of adult mice by Western blot

675 analysis. **(B)** t-SNE plot displaying *TULP2* gene expression pattern during
676 spermatogenesis visualized using published single-cell data(Jung et al., 2019). Black
677 arrow represents the developmental pseudotime corresponding to the developmental
678 ordering of each cell progressing through spermatogenesis. Dot color intensity represents
679 the expression level. Cells from different stages are color-coded. **(C)**
680 Immunofluorescence staining showing TULP2 expression in the cytoplasm of round
681 spermatids (Rs) and elongating spermatids (Es). Scale bars: 5 μm. **(D)** Similar
682 development of adult WT and *TULP2* KO mice. Scale bar: 1 cm. **(E)** Average litter size
683 of pups obtained by fertility test. Each male was caged with two females for 2 months.
684 ***$P < 0.001$, n.s. stands for not significant. **(F)** Similar gross testes morphology, body
685 weight and testis weight between WT and *TULP2* KO mice. Scale bar: 1 mm. n = 4, n.s.
686 stands for not significant. **(G)** Significantly reduced caudal epididymal sperm counts in
687 *TULP2* KO mice compared with WT males. n = 7, ***$P < 0.001$. **(H)** Significantly
688 reduced sperm total motility of *TULP2* KO mice. n = 3, ***$P < 0.001$. Significantly
689 increased abnormal sperm in *TULP2* KO mice (**I** and **J**). Scale bars: 10 μm. n = 3, ***$P <$
690 0.001. **(K)** Electron microscopic analysis displaying ultrastructural defects in *TULP2* KO
691 sperm flagella, including two cross-sections of the same sperm flagellum enclosed within
692 one cell membrane (as shown by red arrowheads), disorganized outer dense fibers and the
693 axonemal microtubules (as shown by red dotted circle). Scale bars: 8 μm (black), 2 μm
694 (red). Error bars depict means ± SEM. All *P*-values were calculated using an unpaired,
695 two-tailed Student's t-test.

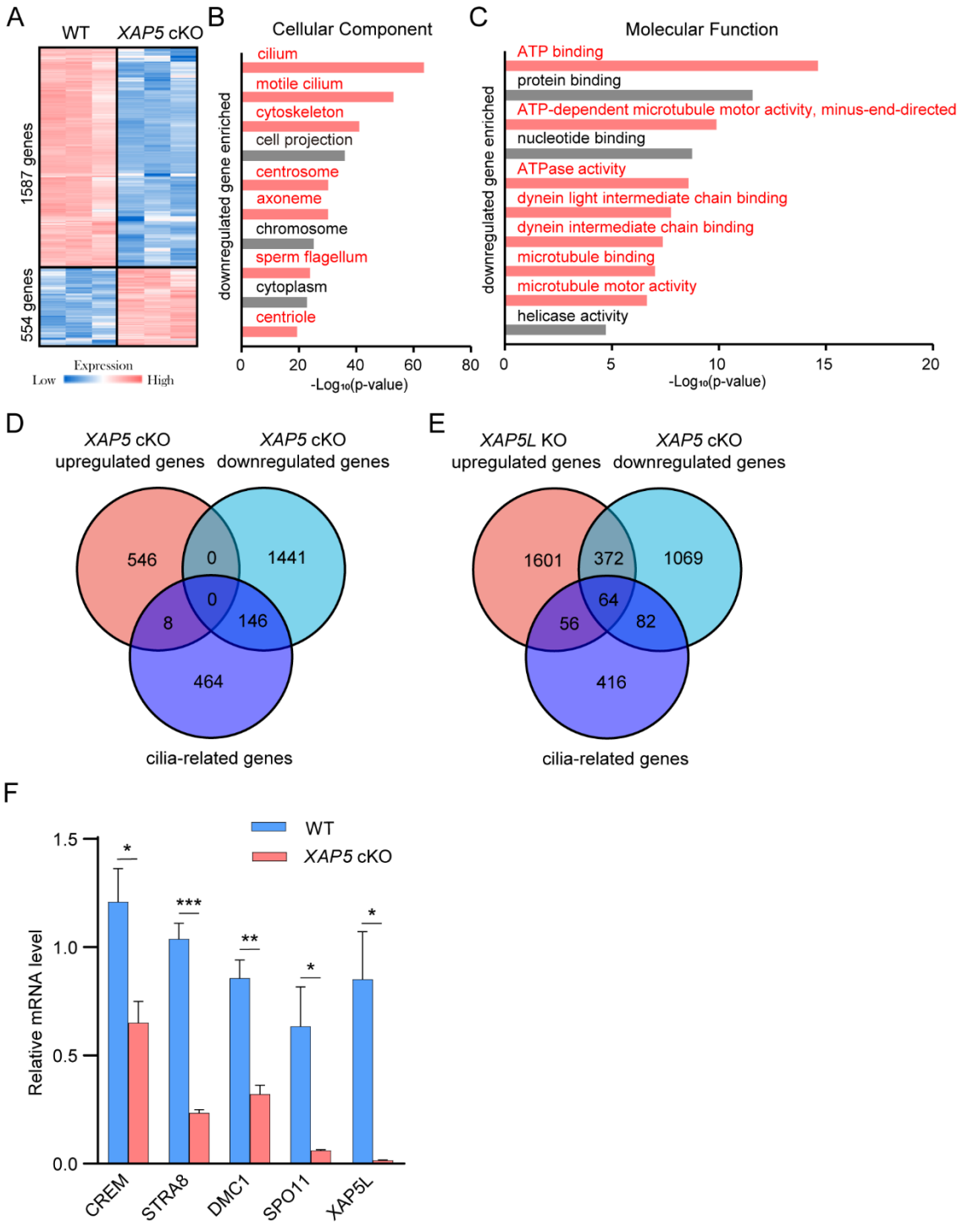

696

697 **Figure S5. XAP5-mediated regulation of ciliary gene expression during mouse**

698 **spermatogenesis.**

699 **(A)** Heat map showing variably expressed genes in P16 *XAP5* cKO testes. Number of

700 related genes was indicated. Gene ontology analysis showing top ten cellular component
701 (**B**) and molecular function (**C**) terms significantly enriched among downregulated genes
702 in *XAP5* cKO testes. **(D)** Venn diagram representing total genes
703 upregulated/downregulated in *XAP5* cKO testes and published cilia-related
704 genes(Nemajerova et al., 2016). **(E)** Venn diagram representing total genes
705 downregulated in *XAP5* cKO testes, upregulated in *XAP5L* KO sperm by at least twofold
706 and published cilia-related genes(Nemajerova et al., 2016). **(F)** Real-time PCR validation
707 of genes involved in ciliogenesis and spermatogenesis. n = 3, **P* < 0.05, ***P* < 0.01, ****P*
708 < 0.001. Error bars depict means ± SEM. All *P*-values were calculated using an unpaired,
709 two-tailed Student's t-test.

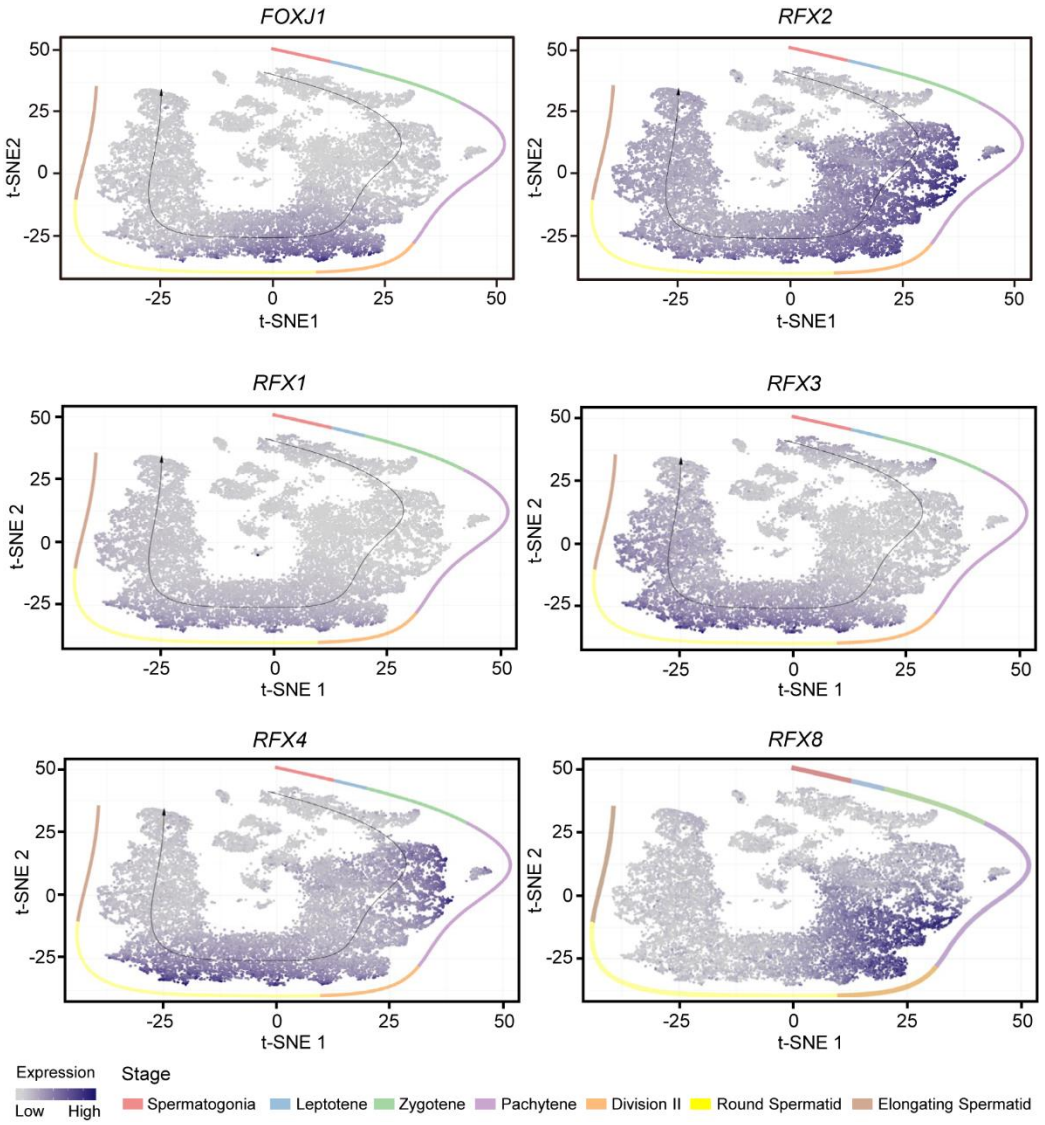

Figure S6. t-SNE plots displaying expression patterns of *FOXJ1* and *RFX* families in individual cell types of mouse testes.

The black arrow represents the developmental pseudotime corresponding to the developmental ordering of each cell progressing through spermatogenesis. Dot color intensity represents the relative expression level. Cells from different stages are color-coded. The gene expression was visualized using the published single-cell data(Jung et al., 2019).